DESY 08-112
Edinburgh 2008/11

The electric dipole moment of the nucleon from simulations at imaginary vacuum angle theta

R. Horsley[1], T. Izubuchi[2,3], Y. Nakamura[4], D. Pleiter[4],
P.E.L. Rakow[5], G. Schierholz[4] and J. Zanotti[1]

[1] *School of Physics, University of Edinburgh, Edinburgh EH9 3JZ, UK*

[2] *Institute for Theoretical Physics, Kanazawa University, Kanazawa, 920-1192 Japan*

[3] *RIKEN-BNL Research Center, Brookhaven National Laboratory, Upton, NY 11973, USA*

[4] *Deutsches Elektronen-Synchrotron DESY,*
John von Neumann-Institut für Computing NIC, 15738 Zeuthen, Germany

[5] *Theoretical Physics Division, Department of Mathematical Sciences,*
University of Liverpool, Liverpool L69 3BX, UK

arXiv:0808.1428v2 [hep-lat] 15 Aug 2008

Abstract

We compute the electric dipole moment of proton and neutron from lattice QCD simulations with $N_f = 2$ flavors of dynamical quarks at imaginary vacuum angle θ. The calculation proceeds via the CP odd form factor F_3. A novel feature of our calculation is that we use partially twisted boundary conditions to extract F_3 at zero momentum transfer. As a byproduct, we test the QCD vacuum at nonvanishing θ.

PACS numbers: 11.30.Er,11.15.Ha,12.38.Gc,13.40.Gp

I. INTRODUCTION

Current measurements of CP violating processes in the K and B meson sector would suggest that the phase of the CKM matrix provides a complete description. However, the baryon asymmetry of the universe cannot be described by this phase alone, suggesting that there are additional sources of CP violation awaiting discovery.

QCD allows for a gauge invariant extra term in the action that is odd under CP transformations,

$$S \to S + i\,\theta\,Q, \tag{1}$$

where Q is the topological charge. Hence, there is the possibility of strong CP violation arising from a nonvanishing vacuum angle θ. The presence of CP violating forces implies a permanent electric dipole moment of the proton and neutron. This attribute is also deeply related to the question of baryon asymmetry of the universe [1].

The current experimental bound on the electric dipole moment of the neutron is [2]

$$|d_N^n| < 2.9 \times 10^{-13}\, e\,\mathrm{fm} \tag{2}$$

($1\,\mathrm{fm} = 10^{-13}\,\mathrm{cm}$). Combining this bound with theoretical estimates of d_N/θ allows us to derive an upper bound on the value of $|\theta|$. Current estimates from QCD sum rules [3] and chiral perturbation theory [4] give $|\theta| \lesssim (1-3) \times 10^{-10}$. This anomaly is known as the strong CP problem.

With the increasingly precise experimental efforts to observe the electric dipole moment of the neutron [5], it is important to have a rigorous calculation directly from QCD.

In this paper we present a calculation of d_N in units of θ with $N_f = 2$ flavors of dynamical quarks using the lattice regularization. The novel feature of our work is that the simulations are performed directly at nonvanishing vacuum angle θ, in contrast to previous lattice studies [6, 7, 8, 9] (with the exception of [10]), which rely on reweighting correlation functions with topological charge that would otherwise vanish. The calculation becomes feasible if θ is rotated to purely imaginary values [11, 12, 13]. We expect from our method a much enhanced signal to noise ratio. In addition, we may hope to gain some insight into the dynamics of the θ vacuum. For a recent review on this matter see [14].

II. THE ACTION

The vacuum angle θ can be rotated into the mass term, in the continuum and on the lattice [15, 16]. This results in the fermionic action

$$S_F = \bar{\psi}\left\{D + \left[\cos(\theta/N_f) + i\,\sin(\theta/N_f)\,\gamma_5\right] m\right\}\psi, \tag{3}$$

where summation over space-time coordinates $\{\vec{x}, t\}$ and quark flavors is understood, and D is the massless Dirac operator. For simplicity, we shall write in the following

$$S_F = \bar{\psi}\left\{D + \bar{m} + i\,(\bar{\theta}/N_f)\,\gamma_5\,\bar{m}\right\}\psi, \tag{4}$$

with

$$\begin{aligned} \bar{m} &= \cos(\theta/N_f)\, m, \\ \bar{\theta} &= \tan(\theta/N_f)\, N_f. \end{aligned} \tag{5}$$

We use clover fermions with $N_f = 2$ flavors of degenerate quarks. Taking into account that chiral symmetry is violated, we then have

$$S_F = \bar{\psi}\left\{D + \bar{m} + i\,(\theta_R/2)\,Z_m^S Z_P\,\gamma_5\,\bar{m}\right\}\psi, \tag{6}$$

where Z_m^S is the *singlet* renormalization constant of the vector Ward identity (VWI) quark mass and Z_P that of the pseudoscalar density, and θ_R is the renormalized vacuum angle,

$$\theta_R = \left(Z_m^S Z_P\right)^{-1}\,\bar{\theta}. \tag{7}$$

It can be shown that Z_P is the same in both the singlet and nonsinglet case, while Z_m is not [17]. Note that $Z_m^S Z_P$ is scale independent, and in the continuum limit $Z_m^S Z_P = 1$ and $\theta_R = \bar{\theta}$.

III. THE SIMULATION

The simulations are performed with the Iwasaki gauge action and said clover fermions with $c_{SW} = 1.47$ on $16^3\,32$ lattices at $\beta = 2.1$, $\kappa = 0.1357$ [18]. The (massless) Dirac operator D in (6) is evaluated at $\kappa_c = 0.138984$. The bare mass is taken to be $a\bar{m} = 1/(2\kappa) - 1/(2\kappa_c)$,

independent of θ. The resulting pion mass is $m_\pi/m_\rho \approx 0.8$, corresponding to a quark mass of $m \approx m_s$, m_s being the strange quark mass. In [18] the lattice spacing in the chiral limit was estimated at $a \approx 0.11$ fm, using the ρ mass to set the scale.

The vacuum angle $\bar{\theta}$ is taken to be purely imaginary,

$$\bar{\theta} = -i\,\bar{\theta}^I, \quad \bar{\theta}^I \in \mathbb{R}, \tag{8}$$

resulting in the action

$$S_F = \bar{\psi}\left\{D + \bar{m} + (\bar{\theta}^I/2)\,\gamma_5\,\bar{m}\right\}\psi. \tag{9}$$

The simulations are done at $\bar{\theta}^I = 0, 0.2, 0.4, 1.0$ and 1.5, where we have collected 9000, 9000, 7000, 6000 and 6000 trajectories of length one, respectively.

We use the highly optimized HMC algorithm of the QCDSF Collaboration [19] for updating the gauge field. After integrating out the Grassmann fields, the action reads

$$S[U,\phi^\dagger,\phi] = S_{\rm G}[U] + S_{\rm det}[U] + \phi^\dagger (Q^\dagger Q)^{-1}\phi, \tag{10}$$

where $S_G[U]$ is the Iwasaki gauge action, $\phi^\dagger$ and ϕ are pseudofermion fields, and

$$\begin{aligned} S_{\rm det}[U] &= -2\,{\rm Tr}\,\log\left(1 + T_{\rm oo} + \frac{\hat{\theta}^I}{2}\,\gamma_5\right), \\ Q &= \left(1 + T + \frac{\hat{\theta}^I}{2}\,\gamma_5\right)_{\rm ee} - M_{\rm eo}\left(1 + T + \frac{\hat{\theta}^I}{2}\,\gamma_5\right)^{-1}_{\rm oo} M_{\rm oe} \end{aligned} \tag{11}$$

with

$$\hat{\theta}^I = \left(1 - \frac{\kappa}{\kappa_c}\right)\,\bar{\theta}^I. \tag{12}$$

$M_{\rm eo}$ and $M_{\rm oe}$ are Wilson hopping matrices, which connect even with odd and odd with even sites, respectively, and T is the clover matrix

$$T = \frac{i}{2} c_{SW}\,\kappa\,\sigma_{\mu\nu} F_{\mu\nu}(x). \tag{13}$$

We apply mass preconditioning à la Hasenbusch [20] and split the resulting action into three parts, each of which we put on separate time scales [21]. We use Omelyan's second order integrator [22] to integrate Hamilton's equations of motion.

IV. RENORMALIZATION

Let us now compute $Z_m^S Z_P$ for our action and coupling, so that we can compare the results to phenomenology later on. We demand that the renormalized VWI and axial vector (AWI) quark masses are equal,

$$m_R = Z_m^S \, m = \frac{Z_A}{Z_P} \, \widetilde{m} = \widetilde{m}_R. \tag{14}$$

That gives $Z_m^S Z_P = Z_A \, \widetilde{m}/m$. At the largest κ value (smallest quark mass) of [18] we find $\widetilde{m}/m = 1.28(2)$. The renormalization constant Z_A has been computed nonperturbatively in [23] for a variety of couplings. Extrapolating the numbers to $\beta = 2.1$ gives $Z_A = 0.78(1)$. Multiplying these two pieces of information together, we obtain $Z_m^S Z_P = 1.00(5)$. That means $\theta_R = \bar{\theta}$ to a good precision.

Alternatively, we may compute $Z_m^S Z_P$ directly from Z_m^S / Z_m^{NS} and $Z_m^{NS} Z_P = Z_P / Z_S^{NS}$. As a comparison, the QCDSF Collaboration, using nonperturbatively improved clover fermions and the plaquette gauge action, finds at $\beta = 5.4$ [17] $Z_m^S / Z_m^{NS} = 1.25(5)$ and [24] $Z_P / Z_S^{NS} = 0.81(2)$. Altogether, this gives $Z_m^S Z_P = 1.01(5)$, in agreement with the CP-PACS result, attesting clover fermions good chiral properties.

V. CHARGE DISTRIBUTION AND θ VACUUM

Before we compute the electric dipole moment now, let us look at the distribution of topological charge and its dependence on θ. Having found that $\theta_R = \bar{\theta}$, the topological charge that follows from the chirally rotated action (3) is the so-called fermionic charge

$$Q = \bar{m} \, \mathrm{Tr} \, \gamma_5 \, M^{-1}, \tag{15}$$

where $M = D + \bar{m}$ is the fermion matrix. The evaluation of (15) requires the computation of the $O(100)$ lowest-lying eigenvalues of M, which is numerically expensive. It has been demonstrated [25, 26, 27] that the fermionic charge and the so-called field theoretic charge, which is computed from the field strength tensor by applying an appropriate number of cooling sweeps and rounding the result to the nearest integer value, give consistent results. In the following we shall employ the field theoretic definition of the topological charge. It

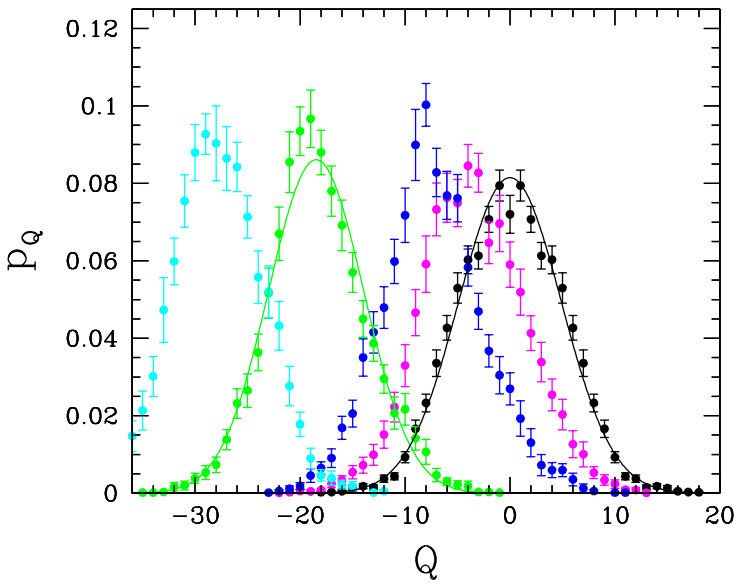

FIG. 1: The topological charge distribution for $\bar{\theta}^I = 0$, 0.2, 0.4, 1.0 and 1.5, from right to left. To guide the eye, the distribution is compared to a Gaussian fit at $\bar{\theta}^I = 0$ and 1.0.

turns out that the results are rather independent of the degree of cooling. In fact, the numbers stabilize already after $O(10)$ cooling sweeps. The numbers quoted here refer to $O(100)$ cooling sweeps. For a recent appraisal of the cooling method see [28].

In Fig. 1 we show the charge distribution for our five different values of $\bar{\theta}^I$. To identify the shape of the distribution, and to see how it changes with increasing value of $\bar{\theta}^I$, we compare our data to a Gaussian fit at $\bar{\theta}^I = 0$ and 1.0. A Gaussian distribution is the most common

$\bar{\theta}^I$	$\langle Q \rangle$	$\langle Q^2 \rangle_c$
0	-0.06(31)	24.9(14)
0.2	-3.52(46)	24.1(15)
0.4	-7.35(36)	22.7(17)
1.0	-18.38(30)	21.7(15)
1.5	-27.84(37)	18.1(13)

TABLE I: The average topological charge and charge squared for our values of $\bar{\theta}^I$.

distribution function for independent, randomly generated variables.

In Table I we present the resulting average topological charge $\langle Q \rangle$ and charge squared,

$$\langle Q^2 \rangle_c \equiv \left\langle (Q - \langle Q \rangle)^2 \right\rangle = \langle Q^2 \rangle - \langle Q \rangle^2, \tag{16}$$

which we plot in Figs. 2 and 3. As with any distribution, besides the distributions mean, its skewness and kurtosis coefficients should be calculated in order to determine the type of distribution. We do so in Figs. 4 and 5, where we plot the skewness S,

$$S = \frac{\langle Q^3 \rangle_c}{\langle Q^2 \rangle_c}, \quad \langle Q^3 \rangle_c \equiv \left\langle (Q - \langle Q \rangle)^3 \right\rangle, \tag{17}$$

and kurtosis K,

$$K = \frac{\langle Q^4 \rangle_c}{\langle Q^2 \rangle_c}, \quad \langle Q^4 \rangle_c \equiv \left\langle (Q - \langle Q \rangle)^4 \right\rangle - 3 \left\langle (Q - \langle Q \rangle)^2 \right\rangle^2. \tag{18}$$

Note that S and K have been normalized to $\langle Q^2 \rangle_c$, different from the mathematical literature, so that the volume dependence cancels out.

Let us first look at the charge distributions in Fig. 1. At $\bar{\theta}^I = 0$ the lattice data show a higher probability than a Gaussian distributed charge for intermediate values of $|Q|$ and a slightly thinner tail, while at larger values of $\bar{\theta}^I$ the distributions appears to show a sharper peak and fatter tail. On top of that, the right tail becomes longer compared to the left one with increasing value of $\bar{\theta}^I$.

This behavior is reflected in the skewness and kurtosis coefficients shown in Figs. 4 and 5. Skewness is a measure of the degree of asymmetry of a distribution. If the right tail of the distribution is more pronounced than the left one, the distribution is said to have positive skewness, which is what we observe at $\bar{\theta}^I > 0$. If the reverse is true, it has negative skewness. Kurtosis is the degree of peakedness of a distribution. A distribution with positive kurtosis is called leptokurtic and has an acute peak around its mean. Examples of leptokurtic distributions include the Laplace distribution. A distribution with negative kurtosis is called platykurtic and has a smaller peak around its mean and a lower probability than a Gaussian distribution at extreme values. Such distributions are termed sub-Gaussian. [1] The kurtosis starts out negative at $\bar{\theta}^I = 0$ and rises almost linearly to reach positive values at $\bar{\theta}^I \gtrsim 0.2$. For recent quenched results see [29, 30, 31].

[1] A distribution $P(x) = \exp[-f(x^2)]$ is called sub-Gaussian if $f'(x^2)$ is strictly increasing on $[0, \infty)$.

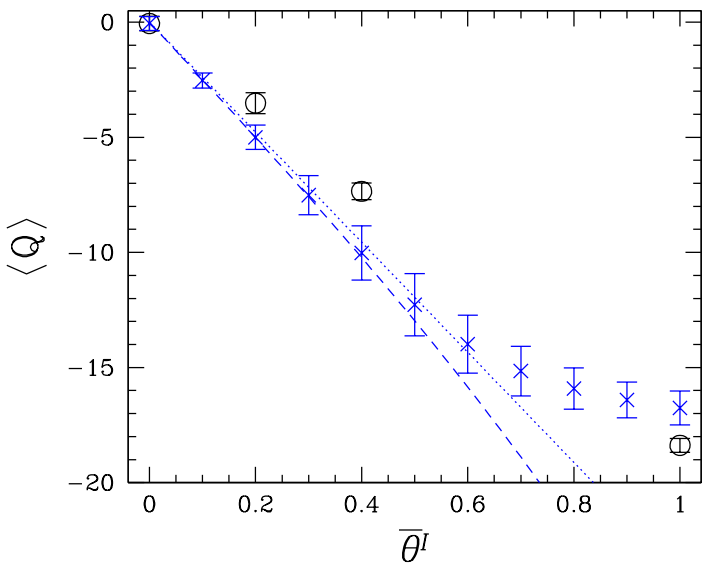

FIG. 2: The average charge (○) compared to the reweighted numbers (×) and to the predictions of the Gaussian distribution (dotted line) and the dilute instanton gas (22) (dashed line).

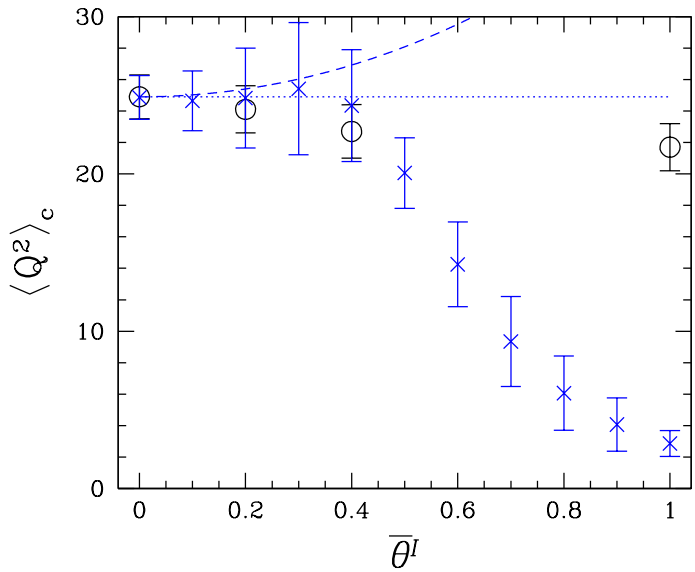

FIG. 3: The average charge squared (○) compared to the reweighted numbers (×) and to the predictions of the Gaussian distribution (dotted line) and the dilute instanton gas (22) (dashed line).

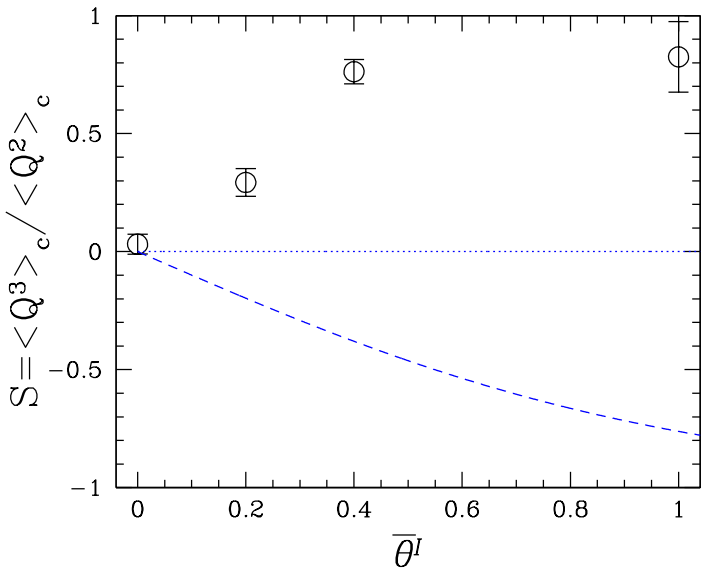

FIG. 4: The skewness compared to the predictions of the Gaussian distribution (dotted line) and the dilute instanton gas (dashed line). The errors shown are the naive ones, as our sample of large charges $|Q - \langle Q \rangle|$ is too small to allow for a proper jackknive analysis, and may be underestimated.

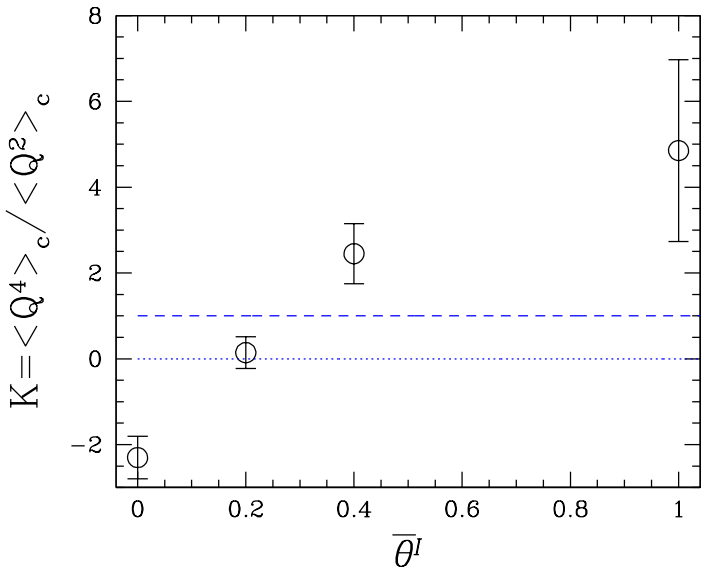

FIG. 5: The Kurtosis, together with its naive error, compared to the predictions of the Gaussian distribution (dotted line) and the dilute instanton gas (dashed line).

A popular model of the QCD vacuum is the dilute instanton gas [32], whose charge distribution is given by a convolution of separate Poisson distributions for instantons and anti-instantons. Its free energy per spacetime volume V is

$$F(\theta) = \chi_t \, (1 - \cos\theta), \quad F(\theta) = -\frac{1}{V} \, \ln \, Z(\theta), \tag{19}$$

where

$$\chi_t = \left. \frac{\langle Q^2 \rangle}{V} \right|_{\theta=0}. \tag{20}$$

That leads to [33]

$$\langle Q^n \rangle_c = -i^n \, V \frac{\partial^n F(\theta)}{\partial \theta^n}, \tag{21}$$

which at imaginary θ gives

$$\begin{aligned} \langle Q \rangle &= -V \chi_t \, \sinh\theta^I, \\ \langle Q^2 \rangle_c &= V \chi_t \, \cosh\theta^I, \\ \langle Q^3 \rangle_c &= -V \chi_t \, \sinh\theta^I, \\ \langle Q^4 \rangle_c &= V \chi_t \, \cosh\theta^I. \end{aligned} \tag{22}$$

In Figs. 2-5 we compare the lattice data for $\langle Q \rangle$, $\langle Q^2 \rangle_c$, S and K with the predictions of the Gaussian distribution and the dilute instanton gas. While $\langle Q \rangle$ and $\langle Q^2 \rangle_c$ are in reasonable agreement with the results of the Gaussian and Poisson distribution for smaller values of $\bar{\theta}^I$, the higher cumulants S and K show a far different trend over the entire range of $\bar{\theta}^I$ than the predictions of these simple models.

Reweighting appears to be the accepted method for simulations at nonvanishing vacuum angle θ and chemical potential μ. Having results of a direct simulation at nonvanishing value of θ at hand, it is instructive to test how reliable the method actually is, given the fact that the simulations are necessarily restricted to a finite volume with limited absolute value of the topological charge.

The reweighted charges are given by

$$\langle Q^n \rangle = \frac{1}{Z(\theta)} \sum_Q Q^n \, P_Q \, \mathrm{e}^{-i\,\theta\,Q}, \quad \sum_Q P_Q = 1, \tag{23}$$

where P_Q denotes the probability of finding a configuration of charge Q in the ensemble of configurations, and

$$Z(\theta) = \sum_Q P_Q \, \mathrm{e}^{-i\,\theta\,Q}. \tag{24}$$

At imaginary $\theta = -i\,\theta^I$ this becomes

$$\langle Q^n \rangle = \frac{1}{Z(\theta)} \sum_Q Q^n\, P_Q\, \mathrm{e}^{-\theta^I\, Q}, \quad Z(\theta) = \sum_Q P_Q\, \mathrm{e}^{-\theta^I\, Q}. \tag{25}$$

In Figs. 2 and 3 we compare $\langle Q \rangle$ and $\langle Q^2 \rangle_c$ with the reweighted numbers, where we have converted θ to $\bar{\theta}$ using (5). On the quantitative level, reweighting is not able to describe the data for $\bar{\theta}^I \geq 0.4$. The reason is that the reweighted charge distributions have largely the same form as the initial $\bar{\theta}^I = 0$ distribution, but are merely shifted towards negative Q values, while the shape of the true charge distributions changes significantly with increasing value of $\bar{\theta}^I$. We may expect to find better agreement on larger volumes, provided $Z(\theta)$ is analytic in θ.

VI. NUCLEON FORM FACTORS AT $\theta \neq 0$

At nonvanishing θ the electromagnetic current between nucleon states can be decomposed in Euclidean space into

$$\langle p', s' | J_\mu | p, s \rangle = \bar{u}_\theta(\vec{p}', s')\, \mathcal{J}_\mu\, u_\theta(\vec{p}, s), \tag{26}$$

with

$$\mathcal{J}_\mu = \gamma_\mu F_1^\theta(q^2) + \sigma_{\mu\nu} q_\nu \frac{F_2^\theta(q^2)}{2m_N^\theta} + \left[(\gamma q\, q_\mu - \gamma_\mu\, q^2)\, \gamma_5\, F_A^\theta(q^2) + \sigma_{\mu\nu} q_\nu\, \gamma_5 \frac{F_3^\theta(q^2)}{2m_N^\theta} \right], \tag{27}$$

where $q = p' - p$. The form factors and nucleon mass will generally depend on θ with $F_{\ldots}^{\theta=0} = F_{\ldots}$ and $m_N^{\theta=0} = m_N$. The Dirac spinors are modified by a phase in the θ vacuum,

$$\begin{aligned} u_\theta(\vec{p}, s) &= \mathrm{e}^{i\alpha(\theta)\gamma_5}\, u(\vec{p}, s), \\ \bar{u}_\theta(\vec{p}, s) &= \bar{u}(\vec{p}, s)\, \mathrm{e}^{i\alpha(\theta)\gamma_5}, \end{aligned} \tag{28}$$

so that the standard spinor relation is modified to

$$\sum_{s',s} u_\theta(\vec{p}, s') \bar{u}_\theta(\vec{p}, s) = \mathrm{e}^{i\alpha(\theta)\gamma_5} \left(\frac{-i\gamma p + m_N^\theta}{2E_N^\theta} \right) \mathrm{e}^{i\alpha(\theta)\gamma_5}. \tag{29}$$

As we are primarily interested in the electric dipole moment in the limit $\theta \to 0$, it is sufficient to consider the lowest order expansion only. Hence, we may write

$$\alpha(\theta) = \alpha'\, \theta + O(\theta^3). \tag{30}$$

For our choice of θ (8), this then becomes to lowest order in θ

$$\sum_{s',s} u_\theta(\vec{p},s')\bar{u}_\theta(\vec{p},s) = \frac{-i\gamma p + m_N(1+2\alpha'\bar{\theta}^I\gamma_5)}{2E_N}. \tag{31}$$

Note that in Euclidean space $q^2 = -(E'-E)^2 + (\vec{p}\,'-\vec{p})^2$ and $\gamma p = iE\gamma_4 + \vec{\gamma}\vec{p}$.

We denote the two-point function of a nucleon of momentum $\vec{p}$ in the theta vacuum by $G^\theta_{NN}(t,\vec{p})$. The phase factor α' of (30) can be obtained from the ratio of two-point functions

$$\begin{aligned} \mathrm{Tr}\,[G^\theta_{NN}(t;0)\Gamma_4] &\simeq \frac{1}{2}|Z_N|^2\,\mathrm{e}^{-m_N t}, \\ \mathrm{Tr}\,[G^\theta_{NN}(t;0)\Gamma_4\gamma_5] &\simeq -\alpha'\bar{\theta}^I\,\frac{1}{2}|Z_N|^2\,\mathrm{e}^{-m_N t}, \end{aligned} \tag{32}$$

where $\Gamma_4 = (1+\gamma_4)/2$. In Fig. 6 we show

$$R(t) = \frac{\mathrm{Tr}\,[G^\theta_{NN}(t,0)\Gamma_4\gamma_5]}{\mathrm{Tr}\,[G^\theta_{NN}(t;0)\Gamma_4]} \simeq -\alpha'\bar{\theta}^I \tag{33}$$

for $\bar{\theta}^I = 0.4$. Fitting to a constant, we find

$\bar{\theta}^I$	$\alpha'\bar{\theta}^I$
0.2	0.048(3)
0.4	0.081(4)

(34)

The form factor $F_3(q^2)$, which is needed for the determination of the nucleon electric dipole moment, can be extracted from the ratio of three-point and two-point functions

$$\begin{aligned} R_\mu(t',t;\vec{p}\,',\vec{p}) &= \frac{G^{\theta\,\Gamma}_{NJ_\mu N}(t',t;\vec{p}\,',\vec{p})}{\mathrm{Tr}\,[G^\theta_{NN}(t';\vec{p}\,')\Gamma_4]} \\ &\quad\times\left\{\frac{\mathrm{Tr}\,[G^\theta_{NN}(t;\vec{p}\,')\Gamma_4]\,\mathrm{Tr}\,[G^\theta_{NN}(t';\vec{p}\,')\Gamma_4]\,\mathrm{Tr}\,[G^\theta_{NN}(t'-t;\vec{p})\Gamma_4]}{\mathrm{Tr}\,[G^\theta_{NN}(t;\vec{p})\Gamma_4]\,\mathrm{Tr}\,[G^\theta_{NN}(t';\vec{p})\Gamma_4]\,\mathrm{Tr}\,[G^\theta_{NN}(t'-t;\vec{p}\,')\Gamma_4]}\right\}^{1/2} \\ &= \sqrt{\frac{E^{\theta\,\prime}\,E^\theta}{(E^{\theta\,\prime}+m^\theta_N)\,(E^\theta+m^\theta_N)}}\,F(\Gamma,\mathcal{J}_\mu), \end{aligned} \tag{35}$$

where $G^{\theta\,\Gamma}_{NJ_\mu N}((t',t;\vec{p}\,',\vec{p})$ is the three-point function, with t' being the time location of the nucleon sink and t the time location of the current insertion, and the function $F(\Gamma,\mathcal{J}_\mu)$ is

$$\begin{aligned} F(\Gamma,\mathcal{J}_\mu) = \frac{1}{4}\,\mathrm{Tr}\,\Gamma\,&\left[\mathrm{e}^{i\alpha(\theta)\gamma_5}\,\frac{E^{\theta\,\prime}\gamma_4 - i\vec{\gamma}\vec{p}\,' + m^\theta_N}{E^{\theta\,\prime}}\,\mathrm{e}^{i\alpha(\theta)\gamma_5}\right] \\ &\times\mathcal{J}_\mu\left[\mathrm{e}^{i\alpha(\theta)\gamma_5}\,\frac{E^\theta\gamma_4 - i\vec{\gamma}\vec{p} + m^\theta_N}{E^\theta}\,\mathrm{e}^{i\alpha(\theta)\gamma_5}\right] \end{aligned} \tag{36}$$

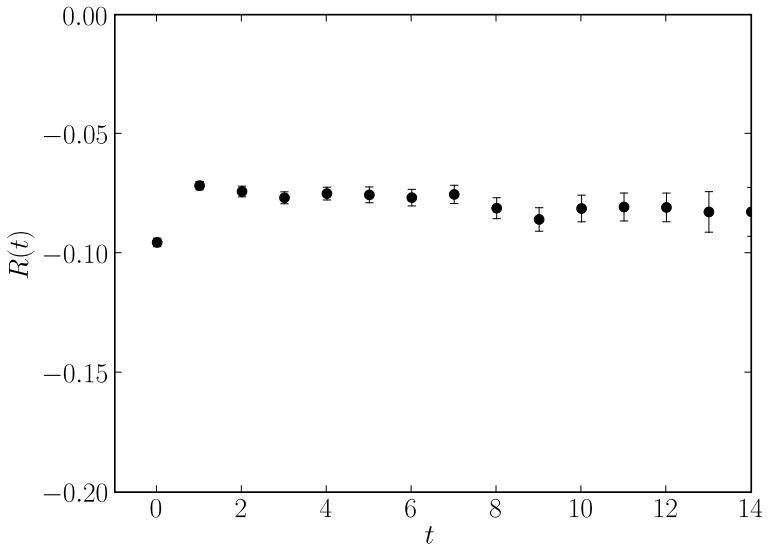

FIG. 6: The ratio $R(t)$ given in (33) for $\bar{\theta}^I = 0.4$.

with $\mathcal{J}_\mu$ given in (27). The three-point functions are calculated for various choices of nucleon polarization, $\Gamma = \Gamma_4$, $i\Gamma_4\gamma_5\gamma_1$ and $i\Gamma_4\gamma_5\gamma_2$. The calculation follows the program of the QCDSF Collaboration [34] for computing nucleon three-point functions. We neglect finite volume corrections to two- and three-point functions [35]. For J_μ we take the local vector current, which needs to be renormalized. We compute the corresponding renormalization constant Z_V [36] from the proton form factor $F_1(0)$ at zero momentum transfer.

With conventional (periodic) boundary conditions momenta are quantized in units of $2\pi/L$, where L is the spatial extent of the lattice. For the lattices used in the current simulation, this means that the smallest nonvanishing momentum available is $\approx 700\,\mathrm{MeV}$. Since F_3 can only be computed at $q^2 \neq 0$, we need to extrapolate to $q^2 = 0$ to find d_N. The momentum resolution of hadron observables can be significantly improved by varying the boundary conditions. It was demonstrated [37] that for processes without final state interactions, such as the form factors studied in this paper, it is sufficient to apply twisted boundary conditions to the valence quarks only.

In our study we use partially twisted boundary conditions, *i.e.* combining gauge field configurations generated with sea quarks with periodic spatial boundary conditions with valence quarks with twisted boundary conditions. The boundary conditions of the valence

quarks attached to the electromagnetic current are

$$\psi(x_k + L) = \mathrm{e}^{i\,\alpha_k}\,\psi(x_k), \quad k = 1, 2, 3. \tag{37}$$

By varying $\vec{\alpha}$ we can tune the momenta of the nucleon continuously. We have chosen the following set of twist angles

$$\begin{aligned} \vec{\alpha} &= \frac{2\pi}{L}\,(0, 0, 0) \\ \vec{\alpha} &= \frac{2\pi}{L}\,(0.36, 0, 0) \\ \vec{\alpha} &= \frac{2\pi}{L}\,(0.36, 0.36, 0) \\ \vec{\alpha} &= \frac{2\pi}{L}\,(0.36, 0.36, 0.36) \end{aligned} \tag{38}$$

The dispersion relation for the nucleon then reads

$$E = \sqrt{m_N^2 + (\vec{p} + \vec{\alpha})^2}. \tag{39}$$

We define the electric dipole moment as

$$d_N^\theta = \frac{e\,F_3^\theta(0)}{2m_N^\theta}. \tag{40}$$

In Fig. 7 we show our results for F_3 for proton and neutron on configutaions with $\bar{\theta}^I = 0.2$ (top) and $\bar{\theta}^I = 0.4$ (bottom). We find a very clean signal for the neutron form factor. The signal for the proton, on the other hand, is somewhat more noisy. The reason is that in this case one has to subtract $F_1^p(0)$ from the matrix element (27), which is by far the largest contribution.

To obtain the result at $q^2 = 0$, we first attempt a fit using a dipole ansatz

$$F_3^\theta(q^2) = \frac{F_3^\theta(0)}{(1 + q^2/M^2)^2}, \tag{41}$$

which is indicated by the solid lines. At $q^2 = 0$ we find

$\bar{\theta}^I$	$F_3^p(0)/(2m_N)$	$F_3^n(0)/(2m_N)$
0.2	0.158(33)	−0.108(17)
0.4	0.256(25)	−0.193(12)

(42)

Alternatively, if we assume that F_3 and F_1^p have similar q^2 behavior, then by forming the ratio

$$\frac{F_3^\theta(q^2)}{F_1^{\theta\,p}(q^2)}, \tag{43}$$

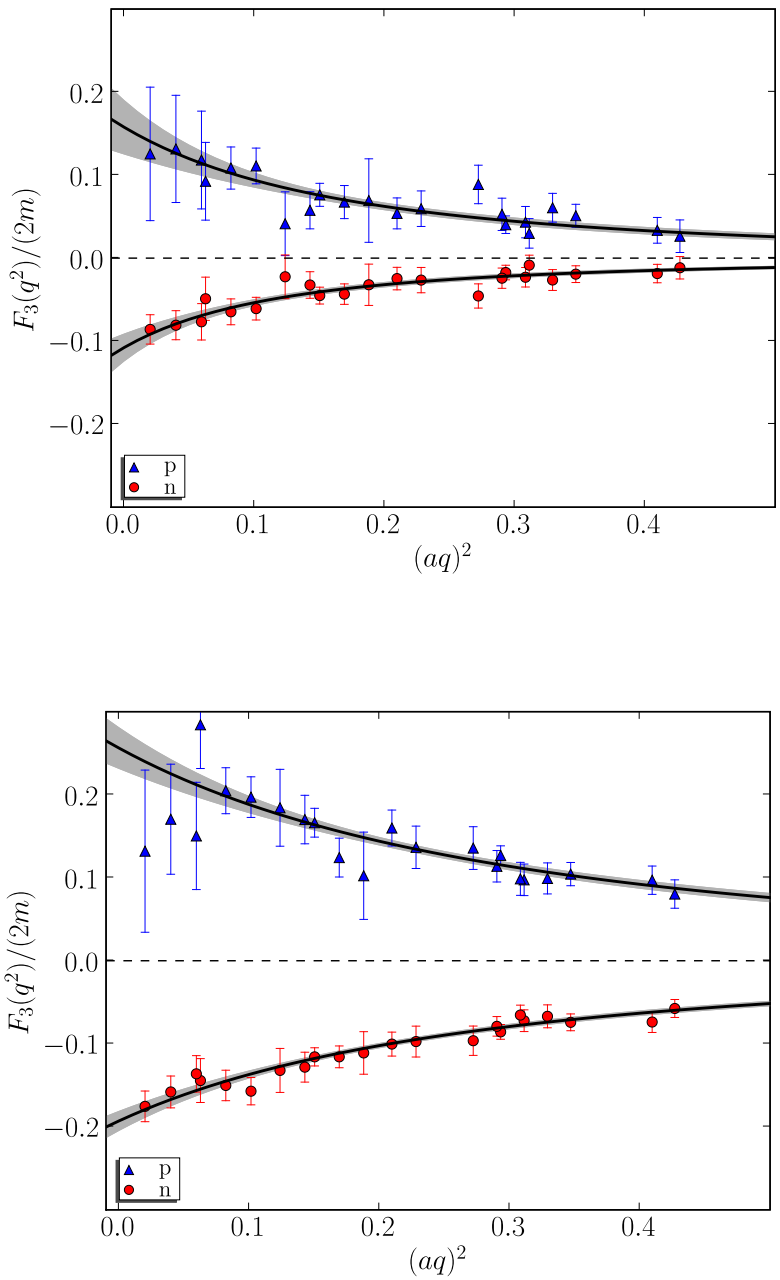

FIG. 7: The form factor $F_3(q^2)$ for proton and neutron, together with a dipole fit, for $\bar{\theta}^I = 0.2$ (top) and $\bar{\theta}^I = 0.4$ (bottom), respectively.

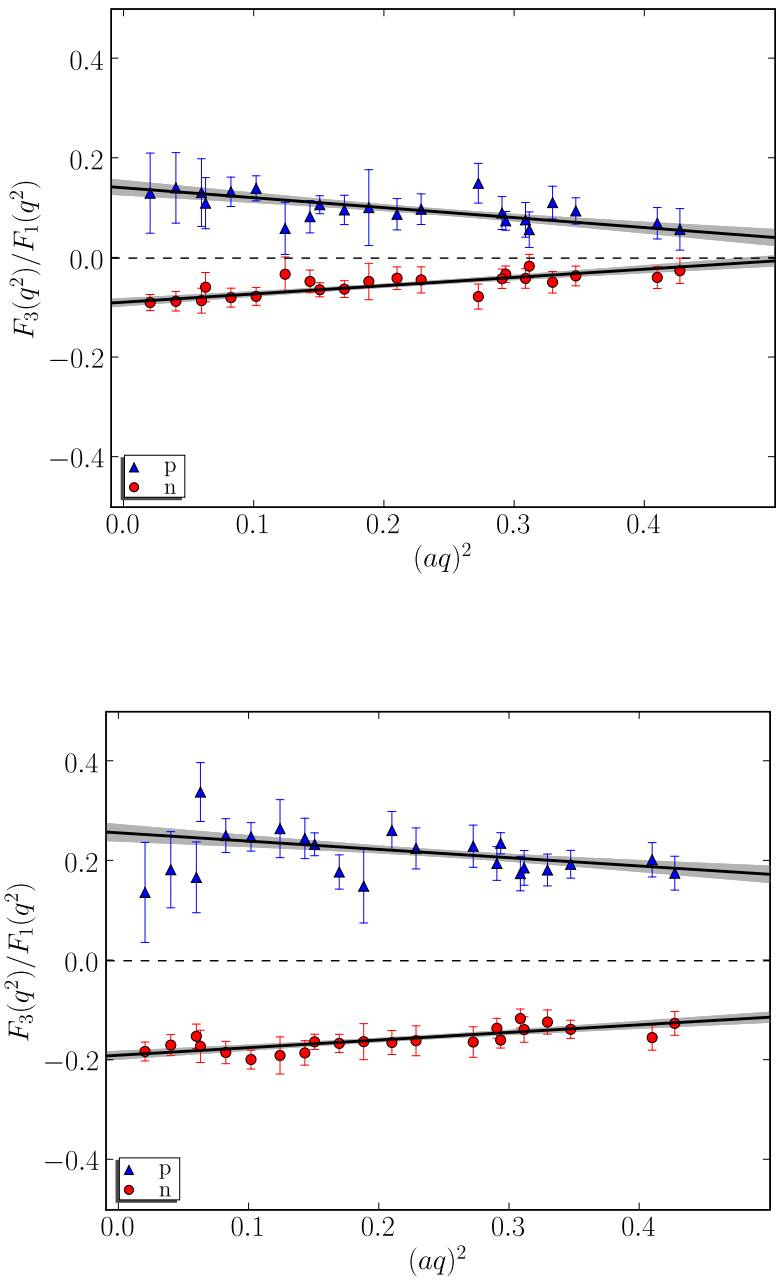

FIG. 8: The form factor ratio $F_3(q^2)/F_1(q^2)$ for proton and neutron, for $\bar{\theta}^I = 0.2$ (top) and $\bar{\theta}^I = 0.4$ (bottom), respectively.

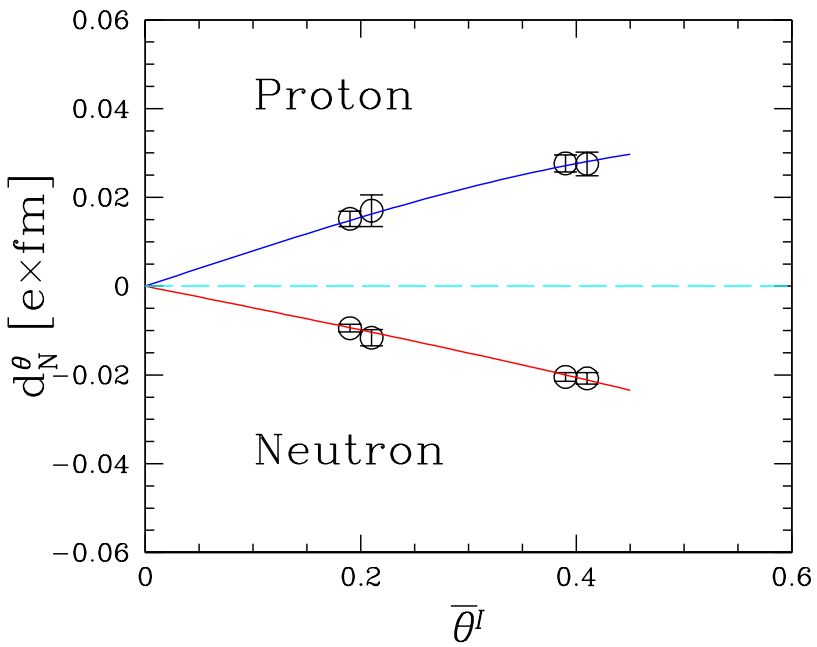

FIG. 9: The electric dipole moment d_N^θ for proton and neutron, together with a linear plus cubic fit. The data points are horizontally displaced for better legibility.

the renormalization constant Z_V cancels, and we may hope to see a constant behavior as a function of q^2. In Fig. 8 we show this ratio. Again, we find a very clean signal for the neutron. After performing a linear extrapolation to $q^2 = 0$, we obtain

$\bar{\theta}^I$	$F_3^p(0)/(2m_N)$	$F_3^n(0)/(2m_N)$
0.2	0.141(16)	−0.088(8)
0.4	0.257(18)	−0.190(9)

(44)

VII. ELECTRIC DIPOLE MOMENT

Both values of $F_3(0)$, (42) and (44), are consistent with each other within the error bars. In Fig. 9 we show the results together with a fit of the form

$$d_N^\theta = \frac{\partial d_N^\theta}{\partial \bar{\theta}^I}\,\bar{\theta}^I + c\,\bar{\theta}^{I\,3}, \tag{45}$$

as we are mainly interested in the derivative $\partial d_N^\theta / \partial \bar{\theta}^I$. The fit gives at $\bar{\theta}^I = 0$

$$\begin{aligned} \frac{\partial d_N^\theta}{\partial \bar{\theta}^I} &= \quad 0.080(10) \;\; [e \times \text{fm}] \quad \text{Proton}, \\ \frac{\partial d_N^\theta}{\partial \bar{\theta}^I} &= -0.049(5) \quad [e \times \text{fm}] \quad \text{Neutron}. \end{aligned} \tag{46}$$

Combining the upper experimental bound on the electric dipole moment of the neutron (2) with our result for $\partial d_N^\theta / \partial \bar{\theta}^I$, we may derive an upper bound on the vacuum angle θ. Taking our results at face value, we find

$$|\theta| < 6 \times 10^{-12}. \tag{47}$$

It should be noted, however, that we are working at unphysically large quark mass yet, so that this result has limited phenomenological significance.

VIII. CONCLUSION AND OUTLOOK

We have performed simulations of QCD with $N_f = 2$ flavors of dynamical quarks at imaginary vacuum angle θ. It is the first time this has been done in full QCD. The use of partially twisted boundary conditions has allowed us to compute the proton and neutron form factor $F_3(q^2)$ with high precision over the entire range of momenta down to $(aq)^2 \approx 0.02$, which greatly facilitated the extrapolation to $q^2 = 0$.

A further improvement of our calculation is that it does not require reweighting of the three-point functions (35) with the topological charge. Barring the fact that the lattice definition of topological charge is ambiguous, to some extent, reweighting does not describe the charge distribution accurately beyond $\bar{\theta}^I > 0.2$, which casts some doubts on the method, if taken at face value.

Having demonstrated the benefit of simulations at imaginary θ, the next step is to extend the calculations to more realistic quark masses and larger lattices. The idea then is to make contact to the predictions of chiral perturbation theory, which allow for the extrapolation of the dipole moment from finite to infinite volume and to the physical quark mass [4, 38]. Chiral perturbation theory also predicts the θ dependence of physical quantities, such as hadron masses. For the pion mass one finds [39]

$$m_\pi^2(\theta) = m_\pi^2(0) \cos(\theta / N_f). \tag{48}$$

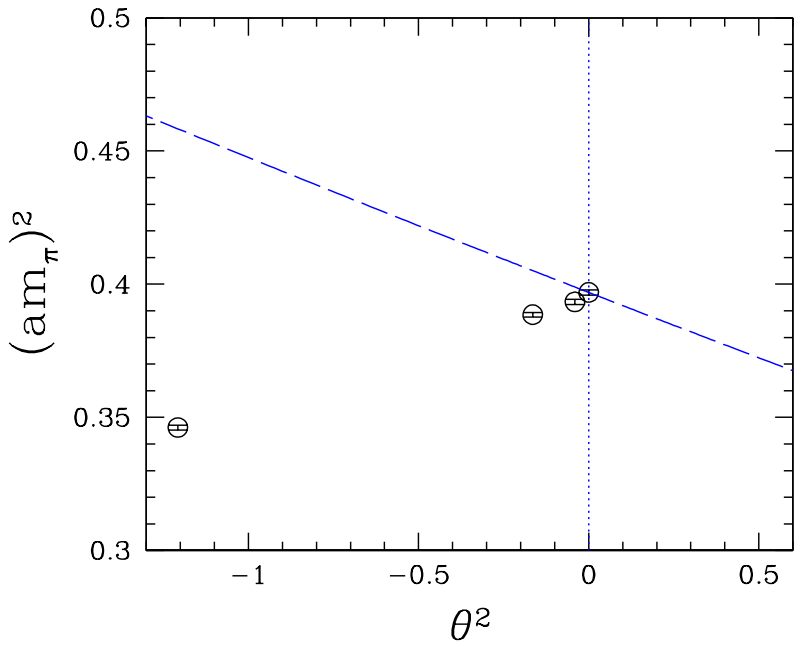

FIG. 10: The pion mass squared as a function of θ squared. The dashed line shows the prediction of chiral perturbation theory.

Though our quark mass is rather heavy, it is tempting to compare our results with (48). This is done in Fig. 10. The variation of m_π with θ is found to be significant. Our results do not confirm the predictions of chiral perturbation theory. It will be interesting to see if this behavior persists at smaller quark masses.

A caveat of our calculation is that clover fermions, though $O(a)$ improved, break chiral symmetry at finite lattice spacing. It is reassuring that $Z_m^S Z_P \approx 1$, which indicates good chiral properties already. But there is the potential danger that the remaining $O(a^2)$ corrections will interfere with the assumed form of the nucleon matrix element (35) and give rise to systematic errors [40]. To fully rule that out, we need to repeat the simulations at smaller lattice spacing. [2]

[2] As an independent check for lattice artifacts, we have repeated the calculation for zero θ angle of the valence quarks on our $\bar{\theta}^I = 0.4$ dynamical background field configurations and found a nonvanishing result for d_N^θ. The result would have been zero in the absence of vacuum insertions of the pseudoscalar density [41].

Finally, we plan to explore a far wider range of θ values, intrigued by the results of a recent simulation of the $O(3)$ nonlinear sigma model in two dimension at imaginary θ [42]. By analytic continuation to real values of θ it was possible to detect the phase transition of the model at $\theta = \pi$ and show that the mass gap vanishes at this point, in agreement with known results [43].

Acknowledgments

We like to thank Wolfgang Bietenholz for carefully reading the manuscript and Luigi Del Debbio for useful discussions. The simulations of the background gauge field have been performed on the BlueGene/L at KEK under the *Large Scale Simulation Program 07-14*, while the analysis and computation of the form factors have been done on the APE computers at DESY Zeuthen. We thank both institutions for their support. This work is supported in part by DFG under contract FOR 465 (Forschergruppe Gitter-Hadronen-Phänomenologie) and 446JAP113/345/0-1 (DFG-JSPS Cooperation Agreement), and by the EU Integrated Infrastructure Initiative Hadron Physics (I3HP) under contract RII3-CT-2004-506078. JZ is supported by STFC Grant PP/D000238/1.

---

[1] M. Trodden, Rev. Mod. Phys. **71**, 1463 (1999) [arXiv:hep-ph/9803479].

[2] C. A. Baker *et al.*, Phys. Rev. Lett. **97**, 131801 (2006) [arXiv:hep-ex/0602020]; C. A. Baker *et al.*, Phys. Rev. Lett. **98**, 149102 (2007) [arXiv:0704.1354 [hep-ex]].

[3] M. Pospelov and A. Ritz, Phys. Rev. Lett. **83**, 2526 (1999) [arXiv:hep-ph/9904483].

[4] B. Borasoy, Phys. Rev. D **61**, 114017 (2000) [arXiv:hep-ph/0004011].

[5] P. G. Harris, arXiv:0709.3100 [hep-ex].

[6] E. Shintani *et al.*, Phys. Rev. D **72**, 014504 (2005) [arXiv:hep-lat/0505022].

[7] E. Shintani *et al.*, Phys. Rev. D **75**, 034507 (2007) [arXiv:hep-lat/0611032].

[8] F. Berruto *et al.*, Phys. Rev. D **73**, 054509 (2006) [arXiv:hep-lat/0512004].

[9] E. Shintani, S. Aoki and Y. Kuramashi, arXiv:0803.0797 [hep-lat].

[10] T. Izubuchi *et al.*, arXiv:0802.1470 [hep-lat].

[11] G. Bhanot and F. David, Nucl. Phys. B **251**, 127 (1985).

[12] V. Azcoiti *et al.*, Phys. Rev. Lett. **89**, 141601 (2002) [arXiv:hep-lat/0203017].

[13] M. Imachi *et al.*, Prog. Theor. Phys. **116**, 181 (2006).

[14] E. Vicari and H. Panagopoulos, arXiv:0803.1593 [hep-th].

[15] E. Seiler and I. O. Stamatescu, Phys. Rev. D **25**, 2177 (1982) [Erratum-ibid. D **26**, 534 (1982)].

[16] W. Kerler, Phys. Rev. D **23**, 2384 (1981).

[17] M. Göckeler *et al.*, Phys. Lett. B **639**, 307 (2006) [arXiv:hep-ph/0409312].

[18] A. Ali Khan *et al.*, Phys. Rev. D **65**, 054505 (2002) [Erratum-ibid. D **67**, 059901 (2003)] [arXiv:hep-lat/0105015].

[19] A. Ali Khan *et al.*, Phys. Lett. B **564**, 235 (2003) [arXiv:hep-lat/0303026]; M. Göckeler *et al.*, PoS **LAT2006**, 160 (2006) [arXiv:hep-lat/0610071]; M. Göckeler *et al.*, PoS **LAT2007**, 041 (2007) [arXiv:0712.3525 [hep-lat]].

[20] M. Hasenbusch, Phys. Lett. B **519**, 177 (2001) [arXiv:hep-lat/0107019].

[21] J. C. Sexton and D. H. Weingarten, Nucl. Phys. B **380**, 665 (1992).

[22] I. P. Omelyan, I. M. Mryglod and R. Folk, Comput. Phys. Commun. 151, 272 (2003).

[23] S. Aoki *et al.*, Nucl. Phys. Proc. Suppl. **106**, 780 (2002) [arXiv:hep-lat/0110128].

[24] M. Göckeler *et al.* [QCDSF Collaboration], in preparation.

[25] T. G. Kovacs, arXiv:hep-lat/0111021.

[26] R. Horsley *et al.*, Nucl. Phys. Proc. Suppl. **106**, 569 (2002) [arXiv:hep-lat/0111030].

[27] R. Horsley *et al.*, Nucl. Phys. Proc. Suppl. **119**, 763 (2003) [arXiv:hep-lat/0211030].

[28] E. M. Ilgenfritz *et al.*, Phys. Rev. D **77**, 074502 (2008) [arXiv:0801.1725 [hep-lat]].

[29] L. Del Debbio, H. Panagopoulos and E. Vicari, JHEP **0208**, 044 (2002) [arXiv:hep-th/0204125].

[30] S. Dürr *et al.*, JHEP **0704**, 055 (2007) [arXiv:hep-lat/0612021].

[31] L. Giusti, S. Petrarca and B. Taglienti, Phys. Rev. D **76**, 094510 (2007) [arXiv:0705.2352 [hep-th]].

[32] C. G. Callan, R. F. Dashen and D. J. Gross, Phys. Rev. D **17**, 2717 (1978).

[33] A. S. Kronfeld *et al.*, Nucl. Phys. B **305**, 661 (1988).

[34] M. Göckeler *et al.*, Phys. Rev. D **53**, 2317 (1996) [arXiv:hep-lat/9508004]; M. Göckeler *et al.*,

PoS **LAT2006**, 120 (2006) [arXiv:hep-lat/0610118].

[35] K. F. Liu, arXiv:0807.1365 [hep-ph].

[36] T. Bakeyev *et al.*, Phys. Lett. B **580**, 197 (2004) [arXiv:hep-lat/0305014].

[37] C. T. Sachrajda and G. Villadoro, Phys. Lett. B **609**, 73 (2005) [arXiv:hep-lat/0411033].

[38] D. O'Connell and M. J. Savage, Phys. Lett. B **633**, 319 (2006) [arXiv:hep-lat/0508009].

[39] R. Brower *et al.*, Phys. Lett. B **560**, 64 (2003) [arXiv:hep-lat/0302005].

[40] S. Aoki *et al.*, Phys. Rev. Lett. **65**, 1092 (1990).

[41] D. Guadagnoli *et al.*, JHEP **0304**, 019 (2003) [arXiv:hep-lat/0210044].

[42] B. Alles and A. Papa, arXiv:0711.1496 [cond-mat.stat-mech].

[43] W. Bietenholz, A. Pochinsky and U. J. Wiese, Phys. Rev. Lett. **75**, 4524 (1995) [arXiv:hep-lat/9505019].